ORIGINAL ARTICLE

Using gravity and topography-implied anomalies to assess data requirements for precise geoid computation

Christopher Jekeli · Hyo Jin Yang · Jay H. Kwon

Abstract Many regions around the world require improved gravimetric data bases to support very accurate geoid modeling for the modernization of height systems using GPS. We present a simple yet effective method to assess gravity data requirements, particularly the necessary resolution, for a desired precision in geoid computation. The approach is based on simulating high-resolution gravimetry using a topography-correlated model that is adjusted to be consistent with an existing network of gravity data. Analysis of these adjusted, simulated data through Stokes's integral indicates where existing gravity data must be supplemented by new surveys in order to achieve an acceptable level of omission error in the geoid undulation. The simulated model can equally be used to analyze commission error, as well as model error and data inconsistencies to a limited extent. The proposed method is applied to South Korea and shows clearly where existing gravity data are too scarce for precise geoid computation.

Keywords Geoid undulation · Data requirements · Gravity–topography correlation

1 Introduction

Height-system modernization using GPS is based on the well-known and simple operative equation that links GPS-derived heights, h, above a given ellipsoid and orthometric heights, H, of a national datum (the same formula holds for normal heights and quasi-geoid undulations or height anomalies):

$$H = h - N, \tag{1}$$

where N is the (local) geoid undulation with respect to the ellipsoid. It is determined from gravimetric data obtained on or near the Earth's surface. Height-system modernization thus depends in the first place on a determination of the required accuracy and resolution of these gravity data. Biases between a global geoid and the local vertical datum and between different ellipsoids can be significant, but are not considered in the present analysis. Our aim is to assess the surface gravity data requirements in order to compute the geoid undulation to a certain desired accuracy.

Apart from errors in the model that relates gravimetric data to the geoid undulation, there are two basic errors that contribute to the total error in the geoid undulation: commission error and omission error. We assume that model errors can be reduced to negligible levels with appropriate theory (see, e.g., Vanicek and Martinec 1994; Sansò and Rummel 1997). However, the commission and omission errors depend largely on the data (and can be affected by methods of data analysis and estimation technique). The commission error results from observational errors that propagate to the computed (or, estimated) geoid undulation; and, the omission error ensues from the discreteness of, or a lack of resolution in the gravimetric data. Both errors can be reduced only with improvements in the data, namely, by reducing observational error and by reducing the data spacing. It is known (and also verified below) that the commission error has much less influence (provided it is strictly random and uncorrelated) than the omission error. The reason is that today's instruments are quite accurate and the data are integrated (summed) to yield

C. Jekeli (✉) · H. J. Yang
Division of Geodesy and Geospatial Science,
School of Earth Sciences, Ohio State University,
Columbus, OH, USA
e-mail: jekeli.1@osu.edu

J. H. Kwon
Department of Geoinformatics, University of Seoul, Seoul, Korea

the geoid undulation; and, summing random errors tends to cancel them. Therefore, we concentrate on the omission error and provide a simple yet effective means to determine the required resolution of gravimetric data in a region, which would support geoid computation to a desired accuracy.

One could approach this problem in a global, or even a regional statistical setting using spectral analyses (e.g., Sjöberg 1979; Schwarz and Li 1996). Indeed, such analyses are quite informative, but, depending on the region of support for the spectrum determinations, they may not be able to distinguish between local areas of relatively rough and smooth gravity signatures. Also, one could assess data requirements on strictly statistical grounds in the space domain, establishing a statistical interpretation of omission errors (of course, this is the standard approach for random commission errors), as done by Kearsley (1986); and, least-squares collocation is another common method for this purpose. However, again, the effect of omission errors depends specifically on the spatial roughness of the field, which may not necessarily be captured accurately by a statistical distribution. For these reasons, it becomes more desirable to perform the analysis using a deterministic approach in the space domain. However, this requires a sufficiently detailed gravity database for the region in question, precisely which may be lacking and whose development depends on the results of the analysis. We show how to simulate such a database from existing data and present an example to establish data requirements for geoid computation.

A high-resolution model of the regional gravity anomaly field may be constructed in the first place from topographic elevation data because of their well-known linear relationship. Such modeling is designed usually for simulation purposes or computational analyses (as in our case) and not for actual field modeling, although the latter certainly has also been employed, particularly for high-degree spherical harmonic models that require uniformly distributed gravity data over the world. It is also known that the linear correlation between gravity anomalies and topography is not perfect and, indeed, it is limited to the short wavelengths. Even here, we may find striking examples where the correlation fails, as in the mid-continent rift region of North America (strongly varying anomalies in essentially flat terrain). Nevertheless, it is a common and largely appropriate method to develop a high-resolution gravity model for the purpose of analyzing its computational properties.

If there exists, in addition, a skeletal network of gravity anomaly data from actual measurements in a region, the question naturally arises how to create a high-resolution regional model using the topographic data in a consistent way. Topographic elevation data usually have much higher resolution and are more easily obtained [e.g., the Shuttle Radar Topography Mission (SRTM) or airborne lidar] than surface or airborne gravity measurements. Combining the gravimetric and topographic data with mutual consistency requires that the individual characteristics of each type are preserved in some way. That is, we wish to ensure that not only the long-wavelength information of the gravity network is maintained, but since each gravity value in the network contains all frequencies, the high-frequency topography-implied gravity anomalies should also fit into the coarse network.

We note that our approach, described below, differs from the recent synthetic gravity field modeling (Baran et al. 2006) that is based on combining long-wavelength spherical harmonic models with short-wavelength topography-implied gravity fields. The long-wavelength information in our case comes primarily from existing gravity data in a region and the topography-implied gravity values are used to fill in the resolution lacking in these data. In this way, the modeling attempts to remain as true as possible to the particular region under study over all frequencies in the field, presenting only a synthesis of the high-resolution field where it is not yet available from actual gravity measurements. A spherical harmonic model limits the spectrum to a certain wavelength and all shorter wavelengths come from just one source, topographic data.

2 Topography-implied anomalies

The first step in combining the gravity anomaly implied by the topographic height, H, and the measured free-air gravity anomaly, Δg, is to develop their theoretical relationship. One form of their putative linear correlation comes from the Bouguer anomaly at a point, P, on or above the Earth's surface, defined by

$$\Delta g_B(P) = \Delta g(P) - 2\pi G \rho H(P) + c(P), \qquad (2)$$

where G is Newton's gravitational constant, ρ is an average density of the topographic mass (the crust), and c is the terrain correction (accounting for the difference between a Bouguer plate assumption and the actual topography in the vicinity of the point). The linear correlation is immediately obvious if we neglect c and consider that the Bouguer anomaly over a particular region tends to be a long-wavelength signal, or approximately constant, $B \approx \Delta g_B$:

$$\Delta g(P) \approx B + 2\pi G \rho H(P). \qquad (3)$$

A second approach for establishing this correlation comes from the theory of isostasy, which attempts to explain the existence of topography on a planet that over time tends toward hydrostatic equilibrium. The isostatic gravity anomaly is given by

$$\Delta g_I(P) = \Delta g(P) - C(P) + A(P), \qquad (4)$$

where $C(P)$ is the gravitational effect of all masses above the geoid and $A(P)$ is the effect of their isostatic compensation.
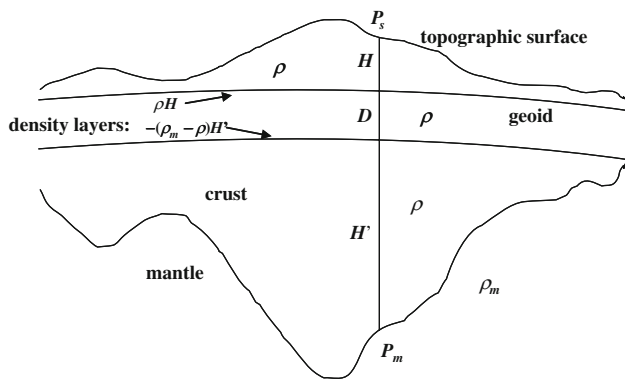
Fig. 1 Isostatic compensation of topography according to the Airy model

Airy's isostasy model supposes that the topography is floating in the mantle in equilibrium according to the buoyancy principle (Fig. 1):

$$\rho H = (\rho_m - \rho)H' = \Delta\rho H', \tag{5}$$

where H' is the (positive) depth of the "root" with respect to the depth of compensation, D (typically, $D = 30\,\text{km}$), and the crust density, ρ, and mantle density, ρ_m, are assumed constant. Similarly, in ocean areas, the lower density of water relative to the crust allows the mantle to intrude into the crust, where equilibrium is established if $(\rho - \rho_w)B = \Delta\rho B'$, and B is the (positive) bathymetric distance to the ocean floor, B' is the height of the "anti-root" of mantle material, and ρ_w is the density of seawater (see Heiskanen and Moritz 1967, p. 136).

Removing the mass that generates $C(P)$ makes the space above the geoid homogeneous (empty). According to Airy's model, the attraction, $A(P)$, is due, in effect, to adding that mass to the root so as to make the mantle homogeneous. If the isostatic compensation is perfect according to this model, then the isostatic anomaly would vanish because of this created homogeneity; and, indeed, isostatic anomalies tend to be small. Therefore, we can model the free-air gravity anomaly, using Eq. (4) with $\Delta g_I(P) \approx 0$, as generated by the attraction due to the topographic masses above the geoid, with density, ρ, and by the attraction due to the (lack of) mass below the depth of compensation, with density, $-\Delta\rho$. We redefine the latter as due to a *negative* density and write:

$$\Delta g(P) \approx C(P) + \bar{A}(P). \tag{6}$$

Expressions for the terms on the right side can be found using various approximations. One approach (Forsberg 1985) is simply to approximate the topography according to its Helmert condensation onto the geoid, whereby its gravitational effect is simulated by a two-dimensional mass layer with density given at a point on the geoid by

$$\kappa_H = \rho H. \tag{7}$$

Similarly, the gravitational effect of the ocean bottom topography can be modeled by forming a layer on the geoid that represents the ocean's *deficiency* in density relative to the crust. The density of this layer is negative: $\kappa_B = -(\rho - \rho_w)B = -\rho(1 - \rho_w/\rho)B$. The potential, V, at a point, P, due to a layer condensed from topography (or bathymetry) is given by

$$V(P) = G\rho R^2 \iint_{\sigma_Q} \frac{\bar{H}(Q)}{s} d\sigma_Q,$$

$$\bar{H}(Q) = \begin{cases} H(Q), & Q \in \text{land} \\ -\left(1 - \frac{\rho_w}{\rho}\right)B(Q), & Q \in \text{ocean} \end{cases} \tag{8}$$

where s is the distance between P and the integration point. The potential and its derivatives (e.g., $C(P) = -\partial V/\partial r_P$, where r_P is the radial coordinate of P) are continuous, as long as P is located above the geoid.

Similarly, the potential (and its derivatives) of the mass added below the depth of compensation can be approximated by that of another layer at level D with density, $\kappa_{H'} = -\Delta\rho H'$, representing a condensation of material that is *deficient* in density with respect to the mantle and extends a depth, H', below D (see Fig. 1). For ocean areas, the anti-root is condensed onto the depth of compensation with density, $\kappa_{B'} = \Delta\rho B'$. Improved approximations of $C(P)$ and $\bar{A}(P)$ certainly may be contemplated (e.g., Makhloof and Ilk 2008; Heck and Seitz 2007; Tsoulis and Stary 2005), as may be the removal of the constant density assumption. However, ignoring these refinements is justified as they are well within the error bounds created by the linear correlation assumption between gravity and topography that is common to all of these modeling methods. Therefore, we adopt the simple Helmert layer model.

Equation (8) for a fixed height of the point, P, is a convolution of H and the inverse distance. Further making the planar approximation (for local applications, as in the present case), this distance becomes

$$s = \sqrt{(x - x')^2 + (y - y')^2 + z^2}, \tag{9}$$

with (x', y') being the local coordinates of points on the geoid. Applying the convolution theorem, the Fourier transform of the potential, Eq. (8), at the level of $z > 0$ is given by

$$\mathcal{F}(V) = \frac{G\rho}{\omega}\mathcal{F}(\bar{H})e^{-2\pi\omega z}, \tag{10}$$

where $\omega = \sqrt{\mu^2 + v^2}$ and μ, v are spatial frequencies corresponding to the plane approximating the geoid.

Including the layer at the compensation depth, D, below the geoid with density, $\kappa_{H'} = -\rho H$ (in view of Eq. (5); and similarly, $\kappa_{B'} = \rho(1 - \rho_w/\rho)B$, for ocean areas), the Fourier transform of the total potential due to both the topography

and its isostatic compensation, is approximately

$$\mathcal{F}(V) = \frac{G\rho}{\omega}\mathcal{F}(\bar{H})(\mathrm{e}^{-2\pi\omega z} - \mathrm{e}^{-2\pi\omega(D+z)}). \tag{11}$$

Consequently, multiplying by $2\pi\omega$ yields the Fourier transform of the gravitational attraction due to these mass layers. Finally, the gravity anomaly (at level $z > 0$) is given by

$$\Delta g = 2\pi G\rho \mathcal{F}^{-1}(\mathcal{F}(\bar{H})(1 - \mathrm{e}^{-2\pi\omega D})\mathrm{e}^{-2\pi\omega z}). \tag{12}$$

We see the same type of linear relationship between the heights and the gravity anomaly as considered in Eq. (3). For the typical compensation depth, $D = 30$ km, the isostatic compensation factor is

$$\mathrm{e}^{-2\pi\omega D} \leq 0.002, \quad \text{for } \omega \geq 3.3 \times 10^{-5} \text{ cy/m}, \tag{13}$$

and could be neglected if the gravity is modeled from topography *only* at resolutions (half-wavelengths) more detailed than $D/2 = 15$ km. However, for larger regions, the isostatic effect should be included. For a practical implementation of formula (12) we use the discrete Fourier transform (DFT), as defined, e.g., in (Brigham 1988, p.97):

$$\Delta g_{j,k} = 2\pi G\rho(\mathrm{DFT}^{-1}((\mathrm{DFT}(\bar{H}))_{\ell,m}$$
$$\times (1 - \mathrm{e}^{-2\pi\omega_{\ell,m}D})\mathrm{e}^{-2\pi\omega_{\ell,m}z}))_{j,k}, \tag{14}$$

where the data are on a regular $J \times K$ grid with intervals, Δx and Δy; and

$$\omega_{j,k} = \sqrt{(\mu_j)^2 + (\nu_k)^2}, \tag{15}$$

$$\mu_j = \begin{cases} \dfrac{j}{J\Delta x}; & j = 0, \ldots, \dfrac{J}{2} - 1 \\ \dfrac{j - J}{J\Delta x}; & j = \dfrac{J}{2}, \ldots, J - 1 \end{cases}$$

$$\nu_k = \begin{cases} \dfrac{k}{K\Delta y}; & k = 0, \ldots, \dfrac{K}{2} - 1 \\ \dfrac{k - K}{K\Delta y}; & k = \dfrac{K}{2}, \ldots, K - 1 \end{cases} \tag{16}$$

and where also $\ell = 0, \ldots, J - 1, m = 0, \ldots, K - 1$.

3 Two-dimensional end-matching

In order to fit the topography-derived (fine-resolution) gravity anomalies to the given (coarse-resolution) network of measured free-air anomalies, we employ a technique that in one dimension amounts to an end-matching algorithm. To fit a one-dimensional profile of fine-resolution anomalies to given values at either end of the profile, we solve for and apply the corresponding bias and trend to the fine-resolution data. In order to extend this idea to two dimensions, we first triangulate the given network of coarse-resolution (CR) data. For example, the Delaunay triangulation is an optimal algorithm that maximizes the minimum angle of each resulting
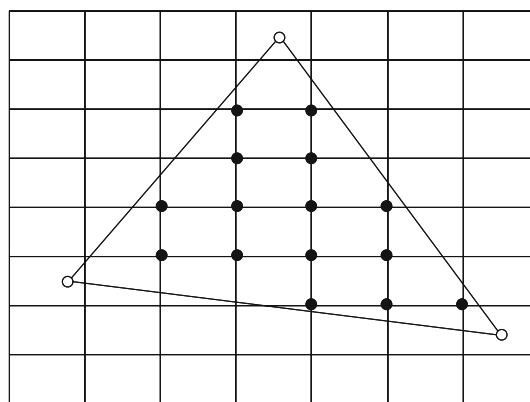
Fig. 2 The fine-resolution data (*solid dots*) on a regular grid and within a triangle defined by coarse-resolution data (*circles*) are adjusted so that the best-fitting plane through them contains the triangle vertices

triangle. Then, we adjust the fine-resolution (FR) data within each triangle such that their best-fitting plane passes through the vertices (measured anomalies) of the triangle (Fig. 2). This is accomplished with the following algorithm.

The equation of a plane is

$$z = \delta + \alpha x + \beta y, \tag{17}$$

where z represents the gravity anomaly data, and (x, y) its planar coordinates. If there are $n > 3$ FR-data points within a triangle, then a least-squares fit of the plane to the anomalies, $\zeta = (z_1 \ldots z_n)^\mathrm{T}$, yields estimates of the parameters, $\xi = (\delta\ \alpha\ \beta)^\mathrm{T}$:

$$\hat{\xi} = (A^\mathrm{T}A)^{-1}A^\mathrm{T}\zeta, \tag{18}$$

where

$$A = \begin{pmatrix} 1 & x_1 & y_1 \\ \vdots & \vdots & \vdots \\ 1 & x_n & y_n \end{pmatrix}. \tag{19}$$

We remove this plane from the FR-data and add the plane implied by the vertices of the CR-triangle, given by

$$\xi_{\mathrm{CR}} = A_{\mathrm{CR}}^{-1}\zeta_{\mathrm{CR}}, \tag{20}$$

where A_{CR} is the analogue of A (Eq. (19)), but for the vertices of the triangle, and ζ_{CR} contains the CR-data at the three vertices. Thus,

$$\bar{z}_k = z_k + (\delta_{\mathrm{CR}} - \hat{\delta}) + (\alpha_{\mathrm{CR}} - \hat{\alpha})x_k + (\beta_{\mathrm{CR}} - \hat{\beta})y_k,$$
$$k = 1, \ldots, n. \tag{21}$$

If $n = 0$, no computation is performed. In case n is 1, 2, or 3, or if the FR-data are co-linear within a triangle, then simply set

$$\bar{z}_k = \delta_{\mathrm{CR}} + \alpha_{\mathrm{CR}}x_k + \beta_{\mathrm{CR}}y_k, \quad k = 1, \ldots, n. \tag{22}$$

In this way, we create a fine-resolution gravity anomaly model from topographic data that is, at the same time, consistent to some degree with the measured gravity anomalies. Measurement errors are not considered, neither in the gravity anomalies nor in the topographic elevations. Although there is an opportunity to incorporate a least-squares weighting based on such random errors, it would not substantially improve the model in most cases (systematic errors or blunders would be much more difficult to identify and remove in this procedure). We also note that least-squares collocation with parameters (the CR-points) could be used to update the FR-data. However, this is basically equivalent to our procedure and was not considered further.

4 Geoid computation

With such a high-resolution gravity anomaly model for a region (that is consistent approximately with existing gravimetric data), one is in a position to determine the required resolution (and accuracy) in gravity data for an accurate geoid determination. For this purpose, we assume that, to first order, the determined resolution is independent of the details associated with the gravity reduction to the geoid when using Stokes's formula (or the Molodensky correction factors when solving the simple Molodensky problem for the telluroid). Similarly, the removal of a longer-wavelength global model (such as EGM96, with resolution of about 30 arcmin) should not influence significantly the required resolution in gravity data, since the needed resolution for a particular geoid accuracy will likely be higher than that of the global model. We may thus consider Stokes's integral of free-air gravity anomalies to represent the geoid undulation exactly for the purpose of the omission (and commission) error analysis. Furthermore, using the same arguments, we may use a planar version of the integral, limited to a local region, E, and supplemented with a global model.

Therefore, with the usual remove/restore procedure, the well-known Stokes's formula for the geoid undulation,

$$N = \frac{R}{4\pi\gamma} \iint_{\sigma} (\Delta g - \Delta g_M) S(\psi) d\sigma + N_M, \qquad (23)$$

becomes

$$N(x, y) = \frac{1}{2\pi\gamma} \iint_{E} \frac{\Delta g(x', y') - \Delta g_M(x', y')}{\sqrt{(x - x')^2 + (y - y')^2}} dx' dy' + N_M(x, y), \qquad (24)$$

where γ is an average value of normal gravity, and Δg_M and N_M are the gravity anomaly and geoid undulation determined from a given global spherical harmonic model. With the FR-data on a $J \times K$ regular grid with data intervals, Δx and Δy, respectively, one may use the DFT approximation of Stokes's integral (the first term in Eq. (24)):

$$\delta N_{\ell,m} = \sqrt{\frac{\Delta x \Delta y}{\pi}} \frac{\delta \Delta g_{\ell,m}}{\gamma} + \frac{\Delta x \Delta y}{2\pi\gamma}$$
$$\times \mathrm{DFT}^{-1}(\mathrm{DFT}(\delta \Delta g)_{j,k} \mathrm{DFT}(\tilde{u})_{j,k})_{\ell,m} \qquad (25)$$

where $\delta \Delta g = \Delta g - \Delta g_M$, and the discrete kernel corresponding to the planar approximation of Stokes's function is

$$u_{\ell,m} = \begin{cases} \frac{1}{\sqrt{\ell^2 \Delta x^2 + m^2 \Delta y^2}}, & \ell \neq 0 \text{ or } m \neq 0 \\ 0, & \ell = 0 \text{ and } m = 0 \end{cases} \qquad (26)$$

and its periodicity is enforced (to comply with the DFT definition) so that

$$u_{\ell+pJ,m+qK} = u_{\ell,m}, \quad \text{for any integers } p, q \qquad (27)$$

In these formulas, $j, \ell = 0, \ldots, J - 1$ and $k, m = 0, \ldots, K - 1$. Note that the singularity in the kernel is accommodated by the first term in Eq. (25) since Stokes's integral is of the weakly singular type. Also, for the practical implementation of these formulas we doubled the extent of the data in both directions with zero padding (Jekeli 1998) to avoid the cyclic convolution error associated with the use of the DFT.

5 An example

The procedure to model the fine-resolution gravity anomaly field from topography and a coarse network of gravity data was applied to data in South Korea. The motivation was to evaluate gravimetric requirements for precise geoid determination in this country. Figure 3 shows the topography (and bathymetry) of the region based on ETOPO2 2 arcmin data. For the simulated gravity anomalies we used 30 arcsec elevation data (but not bathymetry, since it was unavailable at this high resolution), derived from 3 arcsec SRTM data (averages over 30 arcsec × 30 arcsec blocks). The corresponding topography-derived gravity anomalies (denoted as FR-data, Δg_{FR}), according to Eq. (12), are also shown in Fig. 3. For these simulated gravity anomalies, we disregarded the bathymetry by assuming elevations equal to zero ($\bar{H} = 0$) in ocean areas.

Figure 4 depicts over 14,000 stations with gravity data (CR-data, Δg_{CR}) in South Korea. Clearly, the resolution in the north-eastern quadrant is not uniform, with data mostly following existing roads, and the deviation from uniformity is represented by data gaps of the order of 35 km (18 arcmin). In the south-western quadrant, the distribution of data is more uniform and their resolution is roughly 3 km (1.6 arcmin).

An FR-anomaly was interpolated from the FR-grid to each CR-point using inverse distance weighting, and the differences between these two anomalies are shown in Fig. 5. It is clear that the purported linear relationship between gravity anomaly and topography holds reasonably well, since the

Fig. 3 *Left* Topography and bathymetry for Korea mapped from ETOPO2 (2 arcmin) data, with two indicated sub-areas representing relatively smooth and rough terrain. *Right* SRTM topography-implied gravity anomaly for the land area of South Korea
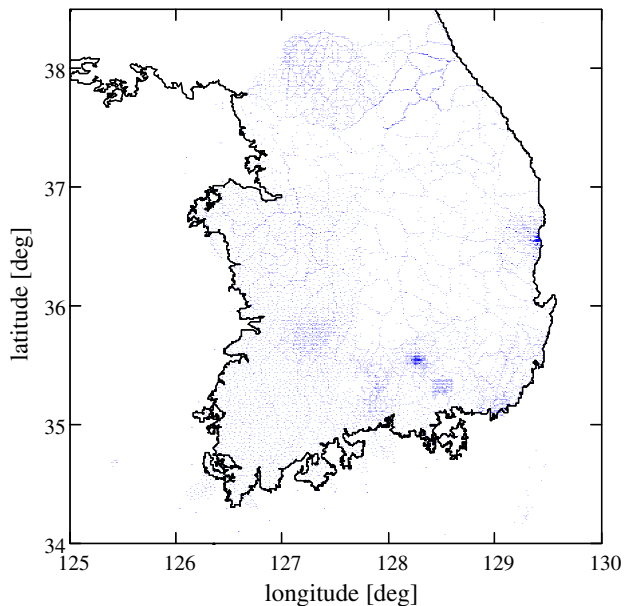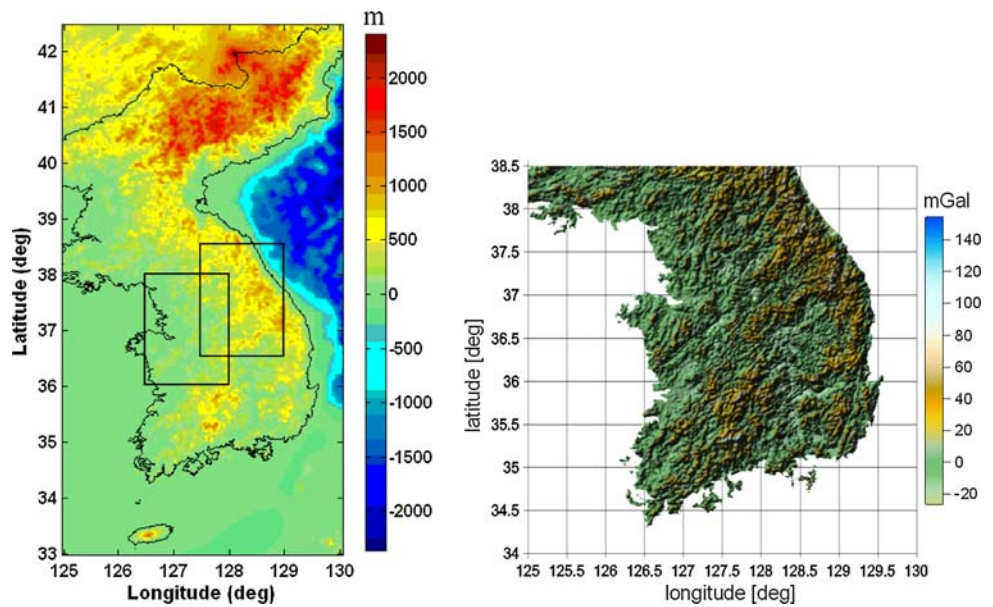

Fig. 4 Locations of existing gravimetric values (CR data)

Fig. 5 Differences between topography-derived anomalies and gravimetric data

differences exhibit near-zero slope with respect to elevation. Table 1 provides some statistics for all anomalies and corresponding comparisons.

Applying the triangulation and plane-matching procedure to these data we obtain a modified, or updated FR-anomaly model ($\overline{\Delta g}_{FR}$). Figure 6 shows profiles of the original FR-data, the CR-data, and the updated FR-model for a representative latitude across South Korea, $\phi = 36°$, containing both high-resolution and low-resolution CR-data. The differences between the updated FR-model interpolated onto the CR-points and the CR-anomalies are shown in Fig. 7, and their statistics are given in Table 1, thus also demonstrating
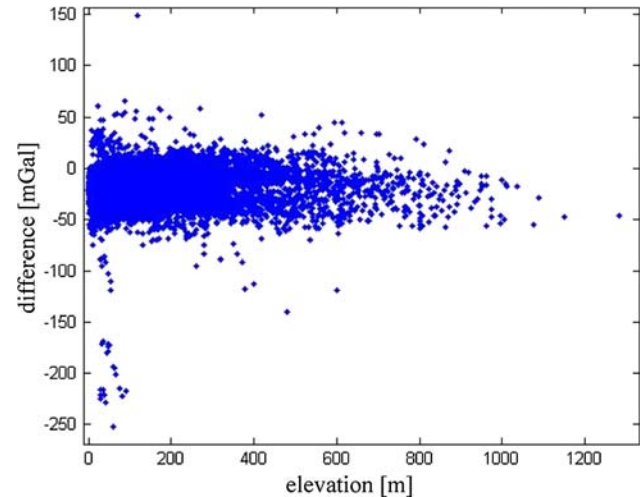
the improvement in the model relative to the existing gravimetric data. The standard deviation of the difference after adjusting the FR-data to the CR-data decreased from 18.6 to 8.7 mGal. A plot of the updated FR-data (Fig. 8) shows, in particular, how the simulated anomaly has been adjusted in the eastern part of the country below the 37° parallel.
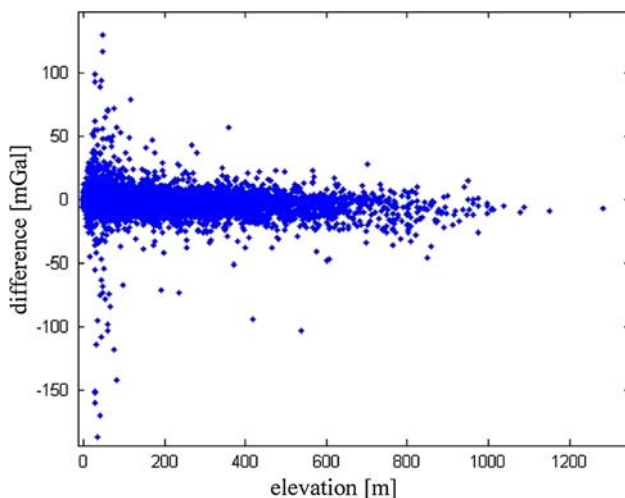
6 Data requirements for geoid determination

The data resolution required to achieve a certain level in the omission error of the geoid undulation is determined by computing the geoid undulations from the simulated gravity data with different levels of decimation. The true geoid
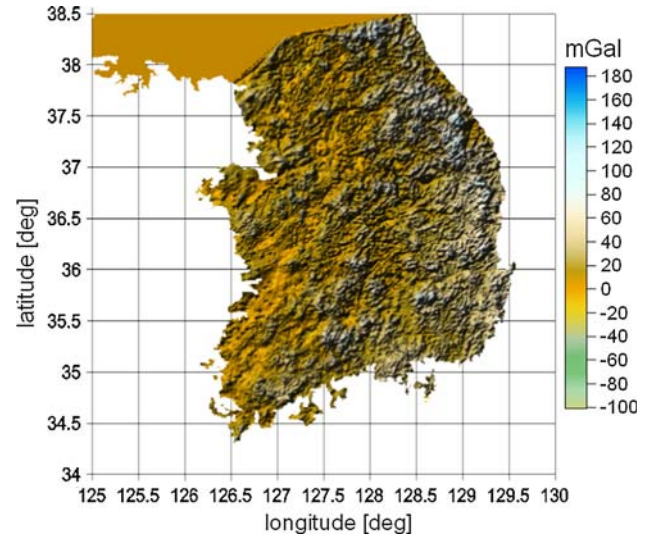
Table 1 Statistics for the anomalies and various comparisons

Quantity	Min	Max	Mean	Std. dev.
Δg_{CR}	−111.13	353.38	23.02	22.43
Δg_{FR}	−26.80	164.15	0.00	16.32
$\overline{\Delta g}_{FR}$	−116.58	210.12	11.31	18.15
$\Delta g_{FR} - \Delta g_{CR}$	−251.70	149.58	−20.21	18.63
$\overline{\Delta g}_{FR} - \Delta g_{CR}$	−186.39	129.64	−1.06	8.67

All values in (mGal)
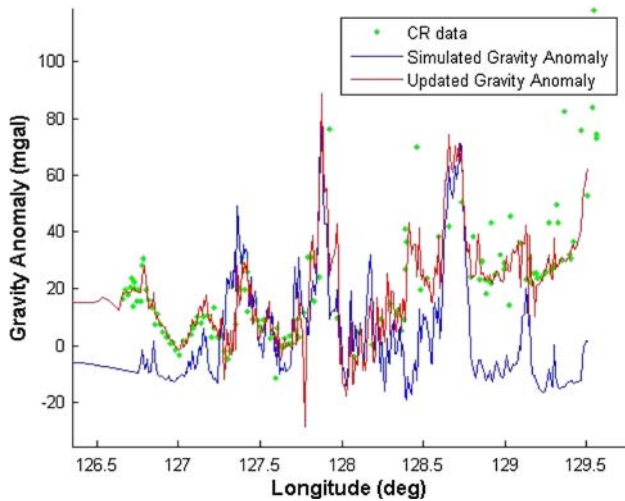
Fig. 6 Profiles of simulated and updated gravity anomalies along the 36° parallel

Fig. 8 SRTM topography-implied gravity anomaly for land area of South Korea, updated by gravimetric data

Fig. 7 Differences between topography-derived, updated anomalies and gravimetric data

undulation is defined by the data with highest resolution, namely the $30'' \times 30''$ $\overline{\Delta g}_{FR}$ data (SRTM topography-implied gravity anomalies fit to existing gravimetric data). These data over the South Korean peninsula were supplemented by extending the $30'' \times 30''$ grid to ocean areas and North Korea (the total area in Fig. 8) with gravity anomalies

computed from the global model EGM08 (Pavlis et al. 2008). Since EGM08 has maximum resolution of $5'$, this extension serves only to mitigate the edge effects in the geoid computation due to the lack of high-resolution data in ocean areas (and gravimetric data in North Korea). Figure 9 shows for one profile in latitude that this extension of data is reasonable across the peninsula as there are no obvious biases and trends in the differences between the simulated and EGM08 anomalies. In general, over the entire region, a similar consistency exists between the simulated land data and the EGM08 model; and, any discrepancies are not expected to influence significantly the values of the determined geoid undulation.

The geoid undulation was computed according to Eqs. (24) and (25) using EGM96 (Lemoine et al. 1998) up to degree and order 180 as the global model, and $\overline{\Delta g}_{FR}$ on $30'' \times 30''$, $1' \times 1'$, $2' \times 2'$, $5' \times 5'$, $7.5' \times 7.5'$, and $10' \times 10'$ grids in the area defined by $34° \leq \phi \leq 38.5°$ in latitude and $125° \leq \lambda \leq 130°$ in longitude (very similar results resulted with EGM96 used up to degree 360). Each set of lower resolution gravity anomalies was derived from the highest resolution by simple decimation. Within this area, we considered two sub-areas representing comparatively smooth and rough topography and corresponding smooth and rough gravity.
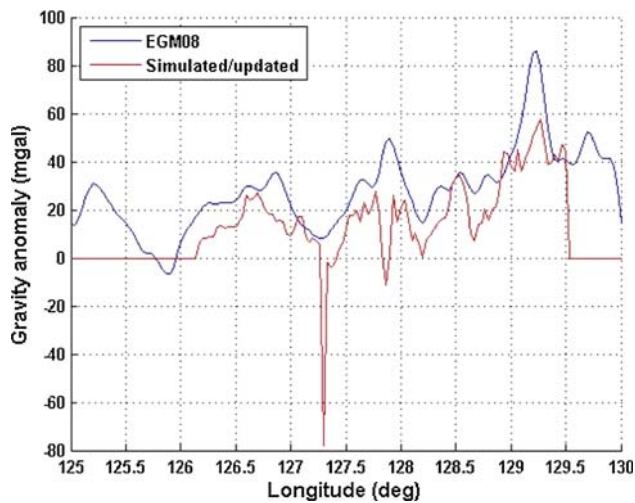
Fig. 9 Profiles of the gravity anomaly at latitude, $\phi = 36.5°$, from EGM08 and from the updated FR-data. The latter is zero by definition over ocean areas

Fig. 10 Root-mean-square of the difference, $N_{\text{estimate}} - N_{\text{true}}$

These areas are shown in Fig. 3, and are delimited in latitude and longitude by $36° \leq \phi \leq 38°$, $126.5° \leq \lambda \leq 128°$, and $36.5° \leq \phi \leq 38.5°$, $127.5° \leq \lambda \leq 129°$, respectively. Within these areas the geoid undulation, N_{est}, for each resolution of data was compared to the true geoid undulation, N_{true}, defined by the highest resolution data. Figure 10 shows the root-mean-square (rms) of the differences.

If the commission and omission errors should contribute equally, then a total rms error of 5 cm would require an omission rms error of 3.5 cm. Therefore, from Fig. 10, in the relatively smooth area, the data resolution should be about 3.5′ (6.5 km); in the rougher area, a bit higher, around 3′ (5.6 km). Clearly, in the southwestern part of South Korea, the gravity data have adequate resolution, whereas, in the northeastern
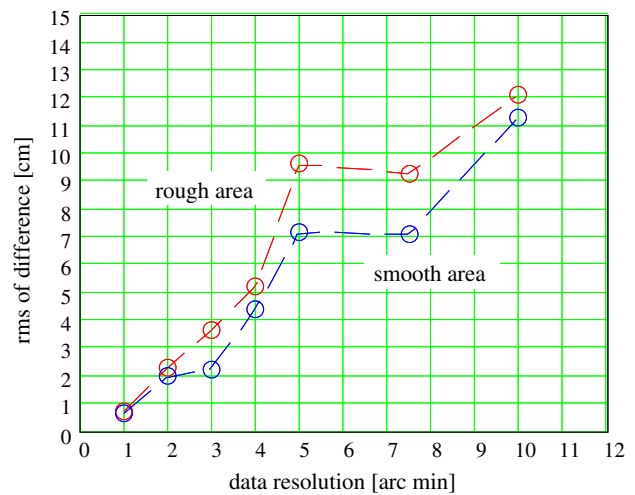
part they do not (see Fig. 4). If the geoid accuracy should be 1 cm (rms), then the omission error (0.7 cm) may be satisfied with data resolution of about 1′ (which would require improved gravimetric resolution in all parts of South Korea). However, this assessment may be somewhat optimistic, since our truth geoid undulation was defined with only twice this resolution. Table 2 provides additional statistics of the geoid differences, $N_{\text{estimate}} - N_{\text{true}}$.

These statistics provide only a summary appraisal of the effect of data resolution on the computed geoid undulation. A more detailed analysis is possible by inspecting individual errors in the spatial domain, as in Fig. 11, which shows the absolute values of the errors when the data resolution is 3 arcmin. The isolated peaks in the error are not necessarily due to low data resolution, and additional analyses (outside the present scope) could be undertaken to determine

Table 2 Statistics of differences, $N_{\text{estimate}} - N_{\text{true}}$, due to limited data resolution; units: (cm)

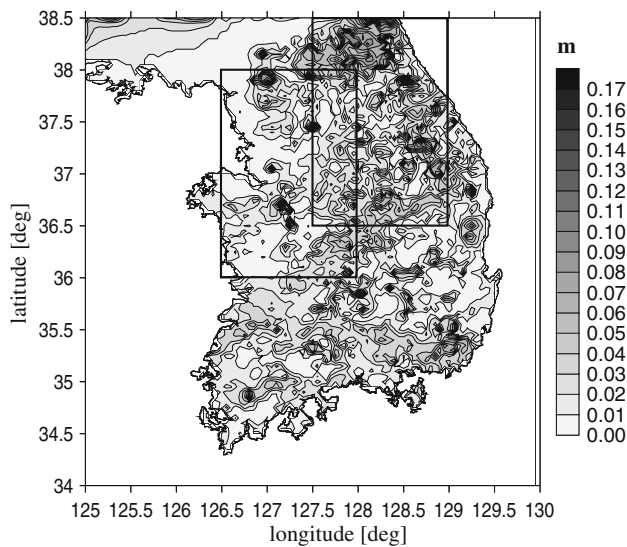| Elevation (m)		Data resolution						
		$1' \times 1'$	$2' \times 2'$	$3' \times 3'$	$4' \times 4'$	$5' \times 5'$	$7.5' \times 7.5'$	$10' \times 10'$
Rough area								
401	Mean	−0.4	0.2	2.0	−3.6	7.6	5.1	3.0
289	Std. dev.	0.7	2.3	3.0	3.7	5.9	7.7	11.7
494	rms	0.7	2.3	3.7	5.2	9.6	9.2	12.1
1,548	Max	3.5	7.6	14.5	11.5	29.2	36.2	46.1
0	Min	−6.0	−12.6	−16.2	−19.2	−10.1	−16.0	−20.9
Smooth area								
162	Mean	−0.5	0.5	0.7	−3.0	4.8	−1.5	2.6
154	Std. dev.	0.5	2.0	2.1	3.3	5.3	6.9	11.0
223	rms	0.6	2.0	2.2	4.4	7.2	7.1	11.3
1,352	Max	4.1	17.0	12.9	10.2	45.7	18.2	56.7
0	Min	−3.7	−5.3	−16.2	−14.1	−12.9	−20.3	−20.9

Fig. 11 Absolute differences, $|N_{\text{estimate}} - N_{\text{true}}|$, for the case of $3' \times 3'$ data resolution

Fig. 12 Triangulation of CR-data near the location of an isolated peak in geoid undulation error. The *white symbols* indicate CR-data greater than 100 mGal or less than −50 mGal

the reason for these peaks and how improved data would reduce them. For example, the peak error near longitude, $\lambda = 127.25°$, and latitude, $\phi = 36.5°$, results from an isolated string of suspiciously large CR-gravity anomalies (100–240 mGal; see Fig. 12), whose effect on the fitting of the FR-data is also evident in the large spike in Fig. 9. Such possibly inconsistent existing data would be candidates for further validation.

Finally, for the sake of completeness, it is easy to determine the commission error due to observation noise in the gravity anomalies, as well as errors in the long wavelength model that is used in the remove/restore process. With standard deviations of simulated (assumed ergodic) Gaussian white noise in the anomalies ranging from 1 to 5 mGal, the propagated random errors in the estimated geoid undulation yield corresponding standard deviations that are almost negligible, as exemplified in Table 3. This verifies the known relative unimportance of measurement error compared to data resolution, provided the former is white noise. Similar results were obtained for other data resolutions. For example, with $4' \times 4'$ resolution, the added random data noise increased the
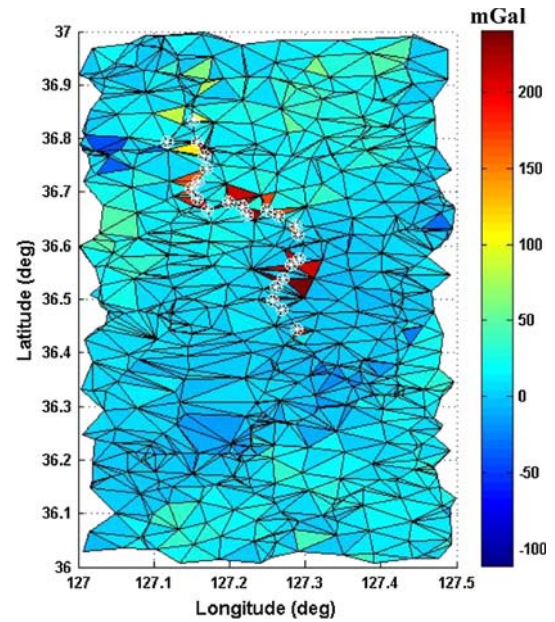
standard deviation in the undulation error from 2.8 cm (no noise) to 2.9 cm (1 mgal noise) and to 3.4 cm (4 mgal noise). Correlated errors, e.g., coming from the spherical harmonic model, have a much more significant effect on the total commission error. Table 3 also lists the error statistics for the estimated undulation if the EGM08 model is used instead of EGM96, both only up to degree 180. The difference in these models for degrees up to 180 may be interpreted as a pseudo-random error in the harmonic coefficients. As shown, the commission error coming from this simulated uncertainty in the global model is much more significant than the effect of uncorrelated noise in the local gravity observations.

7 Conclusions

We have presented a simple yet thorough and comprehensive method to assess gravimetric data requirements for precise geoid computation in a local region such as South Korea.

Table 3 Statistics of differences, $N_{\text{estimate}} - N_{\text{true}}$, due to data noise, $2' \times 2'$ resolution, and simulated errors in the global model, over the entire study area; units: (cm)

Data noise	0 mGal	1 mGal	2 mGal	3 mGal	4 mGal	5 mGal	Harm. coeff. error
Mean	0.31	0.51	0.22	0.65	0.01	1.21	−9.66
Std. dev.	1.33	1.28	1.43	1.71	1.69	1.73	8.60
rms	1.37	1.38	1.45	1.83	1.69	2.11	12.93
Max	16.90	16.60	16.30	17.70	15.90	16.40	15.20
Min	−12.40	−11.80	−13.10	−12.30	−12.20	−10.40	−45.70

The method makes consistent use of both high-resolution topographic elevation data and existing gravimetric data to simulate the field for geoid accuracy analyses. The topographic data, usually available at very high resolution (e.g., from SRTM), are transformed to gravity anomalies on the basis of Airy's isostatic compensation model, further simplified using a Helmert condensation of masses to level surfaces. Matching these high-resolution topography-implied anomalies to existing gravimetric data in the region yields a high-resolution gravity anomaly model that attempts to simulate a densification of the existing network with actual gravimetric data.

Using this method, we showed that certain areas in South Korea, taken as an example, require further gravimetric mapping at high resolution in order to meet specific geoid accuracy requirements, such as 5 or 1 cm (rms). We also showed that gravity data precision, per se, is not nearly as influential (provided it is random); whereas, uncertainty in the global model used in the remove/restore process can be significant. Also, the spatial analysis of the quasi-simulated geoid undulation errors can lead to identification of obvious inconsistencies in the existing data, as demonstrated for one particularly large error.

Finally, it is noted that in areas where the linear correlation between elevation and gravity anomaly breaks down (e.g., in tectonic subduction and rift zones), other modeling will likely be required to assess data requirements for geoid undulation accuracy.

References

Baran I, Kuhn M, Claessens SJ, Featherstone WE, Holmes SA, Vanicek P (2006) A synthetic Earth gravity model designed specifically for testing regional gravimetric geoid determination algorithms. J Geodesy 80(1):1–16

Brigham EO (1988) The fast Fourier transform and its applications. Prentice-Hall, Englewood Cliffs

Forsberg R (1985) Gravity field terrain effect computations by FFT. Bull Géodésique 59(4):342–360

Heck B, Seitz K (2007) A comparison of the tesseroid, prism and point-mass approaches for mass reductions in gravity field modeling. J Geodesy 81(2):121–136

Heiskanen WA, Moritz H (1967) Physical geodesy. W.H. Freeman, San Francisco

Jekeli C (1998) Error analysis of padding schemes for DFT's of convolutions and derivatives. Report no. 446, Geodetic Science, Ohio State University, Columbus, OH. http://geodeticscience.osu.edu/OSUReports.htm

Kearsley AHW (1986) Data requirements for determining precise relative geoid heights from gravimetry. J Geophys Res 91(B9):9193–9201

Lemoine FG, Kenyon SC, Factor JK, Trimmer RG, Pavlis NK, Chinn DS, Cox CM, Klosko SM, Luthcke SB, Torrence MH, Wang YM, Williamson RG, Pavlis EC, Rapp RH, Olson TR (1998) The development of the joint NASA GSFC and the National Imagery and Mapping Agency (NIMA) geopotential model EGM96. NASA Technical Paper NASA/TP-1998-206861, Goddard Space Flight Center, Greenbelt, MA

Makhloof AA, Ilk K-H (2008) Effects of topographic-isostatic masses on gravitational functionals at the Earth's surface and at airborne and satellite altitudes. J Geodesy 82(2):93–111

Pavlis NK, Holmes SA, Kenyon SC, Factor JK (2008) An Earth Gravitational Model to Degree 2160: EGM2008. Presented at the General Assembly of the European Geosciences Union, Vienna, Austria, 13–18 April 2008

Sansò F, Rummel R (eds) (1997) Geodetic boundary value problems in view of the one centimeter geoid. Lecture Notes in the Earth Sciences, vol 65. Springer, Berlin

Schwarz K-P, Li Y (1996) What can airborne gravimetry contribute to geoid determination?. J Geophys Res 101(B8):17873–17881

Sjöberg L (1979) The accuracy of geoid undulations by degree implied by mean gravity anomalies on a sphere. J Geophys Res 84(B11):6226–6230

Tsoulis D, Stary B (2005) An isostatically compensated gravity model using spherical layer distributions. J Geodesy 78(7–8):418–424

Vanicek P, Martinec Z (1994) Stokes–Helmert scheme for the evaluation of a precise geoid. Manuscr Geod 19:119–128